Published May 21, 2007

Caveolin-1 regulates cell polarization and directional migration through Src kinase and Rho GTPases

Araceli Grande-García,[1] Asier Echarri,[1] Johan de Rooij,[2] Nazilla B. Alderson,[1] Clare M. Waterman-Storer,[2] José M. Valdivielso,[1] and Miguel A. del Pozo[1]

[1]Integrin Signaling Laboratory, Department of Vascular Biology and Inflammation, Centro Nacional de Investigaciones Cardiovasculares, 28029 Madrid, Spain
[2]Department of Cell Biology, The Scripps Research Institute, La Jolla, CA 92037

Development, angiogenesis, wound healing, and metastasis all involve the movement of cells in response to changes in the extracellular environment. To determine whether caveolin-1 plays a role in cell migration, we have used fibroblasts from knockout mice. Caveolin-1–deficient cells lose normal cell polarity, exhibit impaired wound healing, and have decreased Rho and increased Rac and Cdc42 GTPase activities. Directional persistency of migration is lost, and the cells show an impaired response to external directional stimuli. Both Src inactivation and p190RhoGAP knockdown restore the wild-type phenotype to caveolin-1–deficient cells, suggesting that caveolin-1 stimulates normal Rho GTP loading through inactivation of the Src–p190RhoGAP pathway. These findings highlight the importance of caveolin-1 in the establishment of cell polarity during directional migration through coordination of the signaling of Src kinase and Rho GTPases.

Introduction

Cell migration is a key step in many physiological and pathological processes, such as wound repair, embryonic development, tissue regeneration, angiogenesis, and metastasis (Ridley et al., 2003; Vicente-Manzanares et al., 2005). In an attempt to understand this complex process, migration has been viewed as a multiple-step cycle, where migrating cells become highly polarized and display sequential morphological changes (Sheetz et al., 1999; Ridley et al., 2003). These include extension of protrusions at the cell front, formation of stable adhesions at the leading edge, reorientation of the Golgi and the microtubule organizing center (MTOC) toward the leading edge, translocation of the cell body in the direction of the movement, and focal adhesion (FA) release and retraction at the cell rear (Vicente-Manzanares et al., 2005). These steps are easily observed in slow-moving cells, such as fibroblasts and endothelial cells (Ridley et al., 2003). The acquisition of a highly polarized phenotype is not generally regarded as a step in the migration process but, rather, as a concomitant and essential event to cell migration (Sánchez-Madrid and del Pozo, 1999; Vicente-Manzanares et al., 2005).

Migration is a very complex process that requires the spatial and temporal integration of different signaling components (for reviews see Ridley et al., 2003; Vicente-Manzanares et al., 2005), many of which are not yet understood. Among them, the Rho family of small GTPases is one of the master regulators of cell motility, as they control both actin cytoskeleton remodeling as well as FA formation and turnover. FAs are one of the key elements in migration (Geiger and Bershadsky, 2001; DeMali et al., 2003; Ridley et al., 2003; Carragher and Frame, 2004; Vicente-Manzanares et al., 2005). They are formed by the recruitment of cytoskeletal and signaling proteins to the sites where integrins attach to the ECM. FAs serve as anchorage points for stress fibers (Wehrle-Haller and Imhof, 2002; Carragher and Frame, 2004). Highly regulated, polarized actin polymerization is involved in the protrusion formation at the leading edge of the cell, whereas detachment and retraction of the cell rear involves myosin-dependent contraction of stress fibers in the tail (Ridley et al., 2003; Vicente-Manzanares et al., 2005). Both FAs and stress fibers are regulated by Rho GTPases. By coordinating the activation of several effectors and, ultimately, actin polymerization, Cdc42 triggers filopodia and Rac regulates lamellipodia

Correspondence to Miguel A. del Pozo: madelpozo@cnic.es

J. de Rooij's present address is Netherlands Cancer Institute, 1066 CX Amsterdam, Netherlands.

J.M. Valdivielso's present address is Hospital Universitario Arnau de Vilanova, Universidad de Lleida, 25198 Lleida, Spain.

Abbreviations used in this paper: Csk, C-terminal Src kinase; EF, elliptical factor; FA, focal adhesion; Fn, fibronectin; ID, index of directionality; MEF, mouse embryonic fibroblast; MTOC, microtubule organizing center; shRNA, short hairpin RNA; WT, wild-type.

The online version of this article contains supplemental material.

Supplemental Material can be found at:
/content/suppl/2007/05/18/jcb.200701006.DC1.html

The Journal of Cell Biology, Vol. 177, No. 4, May 21, 2007 683–694
http://www.jcb.org/cgi/doi/10.1083/jcb.200701006

Published May 21, 2007

protrusion and membrane ruffles, whereas Rho regulates formation of stress fibers and cell contractility in the cell body, and hence Rho activity is high at the cell contractile tail (Raftopoulou and Hall, 2004; Vicente-Manzanares et al., 2005). Importantly, it has recently been reported that Rho activity is also high at a sharp band immediately adjacent to the leading edge of cells migrating out of a wounded monolayer (Kurokawa and Matsuda, 2005; Pertz et al., 2006). On the other hand, Rac and Cdc42 regulate the initial recruitment of cytoskeletal and signaling proteins into small focal complexes, whereas Rho controls the maturation of these complexes into bigger FAs, as well as FA lifetime (Rottner et al., 1999; Burridge and Wennerberg, 2004; Raftopoulou and Hall, 2004; Vicente-Manzanares et al., 2005).

Many other players are involved in the complex regulation of cell migration (Ridley et al., 2003; Vicente-Manzanares et al., 2005), among them, caveolae and caveolin (Navarro et al., 2004), although in a controversial manner. Caveolae are specialized plasma membrane microdomains with a flask-shaped, invaginated morphology, highly enriched in cholesterol and sphingolipids (Parton et al., 2006). Caveolin is their principal structural component. There are three proteins encoded by the caveolin gene family (caveolin-1, -2, and -3). Caveolin-1 and -2 are coexpressed in numerous cell types, whereas caveolin-3 is muscle specific. It has been proposed that caveolin-1 could play an important role in cell motility by controlling polarization of signaling molecules (Shaul and Anderson, 1998; Isshiki et al., 2002). Supporting this notion, caveolin-1 is linked to the actin cytoskeleton through filamin (Stahlhut and van Deurs, 2000) and has been proposed to associate with a certain subset of integrins (Wary et al., 1998; Wei et al., 1999). On the other hand, caveolin-1 and caveolae present a polarized distribution in migrating endothelial cells (Parat et al., 2003; Beardsley et al., 2005). Moreover, several reports have shown that migration is affected by changes in caveolin-1 expression levels, although in a controversial manner. Some data suggest that caveolin-1 promotes cell migration. Thus, knock down of caveolin-1 expression correlated with a decrease in the chemotaxis of endothelial cells, astrocytes, and multiple myeloma cells (Galvez et al., 2004; Ge and Pachter, 2004; Podar et al., 2004). However, other studies indicate that caveolin-1 could be a negative regulator. For instance, restoration of caveolin-1 expression in MTLn3 cells reduces lamellipodia formation and chemotactic migration (Zhang et al., 2000). Likewise, caveolin-1 knockdown increased directed migration toward sphingosine-1 phosphate in bovine aortic endothelial cells (Gonzalez et al., 2004). Although some of these discrepancies could be ascribed to technical or cell type specificity issues, it seems important to ascertain what kind of role, if any, caveolin-1 plays in the coordinated processes of polarization and migration. We decided to explore this issue by using fibroblasts from caveolin-1–deficient mice. These cells do not express any caveolins, as caveolin-2 is degraded in the absence of caveolin-1 through the proteasomal pathway (Razani et al., 2001), and caveolin-3 is muscle specific. Our results demonstrate that caveolin-1 plays an essential role in the acquisition of a polarized phenotype and, accordingly, in directional cell migration, including both intrinsic persistence of migration and chemotaxis. It does so by regulating the activation of Src, which in turn regulates signaling by Rho GTPases.

Results

Caveolin-1 is required for the acquisition of a normal polarized phenotype in fibroblasts

We compared the morphological phenotype of wild-type (WT) and caveolin-1–deficient mouse embryonic fibroblasts (MEFs; Razani et al., 2001) spread on fibronectin (Fn) by immunofluorescence confocal analysis. As shown in Fig. 1 a, Cav1$^{-/-}$ MEFs displayed a remarkable morphological change. Most of the WT MEFs exhibited a polarized morphology, with an elongated, polygonal shape (see Fig. 7 g, left). However, Cav1$^{-/-}$ MEFs adopted a nonpolarized, rounded shape and displayed an aberrant architecture of the actin cytoskeleton. Stress fibers presented a peripheral, concentric localization, creating cortical

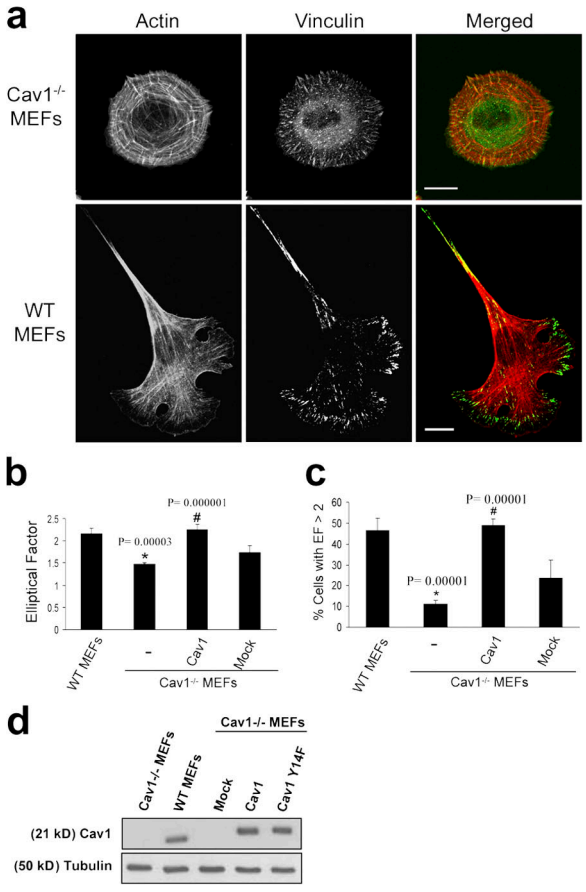

Figure 1. **Cav1$^{-/-}$ MEFs show a defect in stress fiber architecture and FAs.** (a) WT and Cav1$^{-/-}$ MEFs were plated on Fn, fixed, and stained with rhodamine phalloidin to reveal the morphology of the actin cytoskeleton. FAs were stained with a mAb to vinculin followed by FITC-conjugated anti-rabbit IgG. Bars, 20 μm. (b) The EF (length/breadth), used as a measure of cell polarization, was calculated for WT MEFs (n = 797), Cav1$^{-/-}$ MEFs (n = 663), Cav1-reconstituted knockout MEFs (n = 481), and knockout MEFs stably transfected with the empty vector (mock; n = 450) plated on Fn. Error bars indicate SEM from five separate experiments. (c) The percentage of cells with EF >2 was calculated for each cell line. Error bars indicate SEM. (d) WT MEFs, Cav1$^{-/-}$ MEFs, and Cav1$^{-/-}$ MEFs reconstituted with empty vector (mock), caveolin-1, or caveolin-1 Y14F were lysed and immunoblotted against caveolin-1 and tubulin. Exogenous caveolin-1 is flag tagged.

Published May 21, 2007

actin ring structures, whereas in WT MEFs, stress fibers were organized in bundles aligned along the long axis of the cell. We also detected an alteration in the formation of vinculin-stained FAs. These structures were smaller, much like focal complexes (Geiger and Bershadsky, 2001), and more abundant compared with normal fibroblasts. In addition, adhesions were distributed over the entire ventral surface, whereas in WT MEFs, FAs were mostly located at cell edges. Interestingly, Cav1$^{-/-}$ MEFs presented abundant homogeneously distributed vinculin, i.e., not associated with adhesive complexes (Fig. 1 a, top middle), consistent with the altered, immature focal complexes phenotype observed in these cells. Paxillin staining was very similar to that of vinculin (see Fig. 7 g and Fig. S4, available at http://www.jcb.org/cgi/content/full/jcb.200701006/DC1). To quantify morphological changes detected in Cav1$^{-/-}$ MEFs, we calculated the elliptical factor (EF), which is defined as the ratio between the longest and the shortest axis in the cell. In WT MEFs, EF was significantly higher than that of Cav1$^{-/-}$ MEFs (Fig. 1 b). Importantly, a much higher WT population displayed an EF >2 (indicative of a polarized morphology) compared with the Cav1$^{-/-}$ population (Fig. 1 c). Similar results were obtained with fibroblasts prepared from a Cav1 conditional knockout mouse (Valasek et al., 2005) versus their WT littermates (see Fig. 7 g, bottom; quantified in Fig. S3, b and c) . Fibroblasts prepared from these two strains of Cav1$^{-/-}$ mice (Razani et al., 2001; Valasek et al., 2005) have been used throughout this study. Cell area measurements showed that Cav1$^{-/-}$ cells do not exhibit a delay in cell spreading, and the morphological changes described were still present at late time points after spreading (Fig. S1). Reexpression of caveolin-1 in Cav1$^{-/-}$ MEFs (Fig. 1 d) restored the normal EF (Fig. 1, b and c; and see Fig. 7 g), thus showing that caveolin-1 is required for elongation. Altogether, these results suggest that caveolin-1 is required for the acquisition of an elongated morphology, stress fiber architecture, and FA formation in fibroblasts.

Polarization usually correlates with, but is not equivalent to, elongation. To directly measure cell polarity stimulated by a directional stimulus, we assayed for MTOC polarization in fibroblasts migrating out of a wounded monolayer. MTOC reorientation toward the leading edge was substantially reduced in Cav1$^{-/-}$ MEFs, and Cav1 reexpression restored polarity to levels achieved in WT cells (Fig. 2 a; quantified in Fig. 2 b). Collectively, these results demonstrate a defect in the establishment of cell polarity in the caveolin-1–deficient fibroblasts and establish a correlation between elongation defects and polarization changes in these cells.

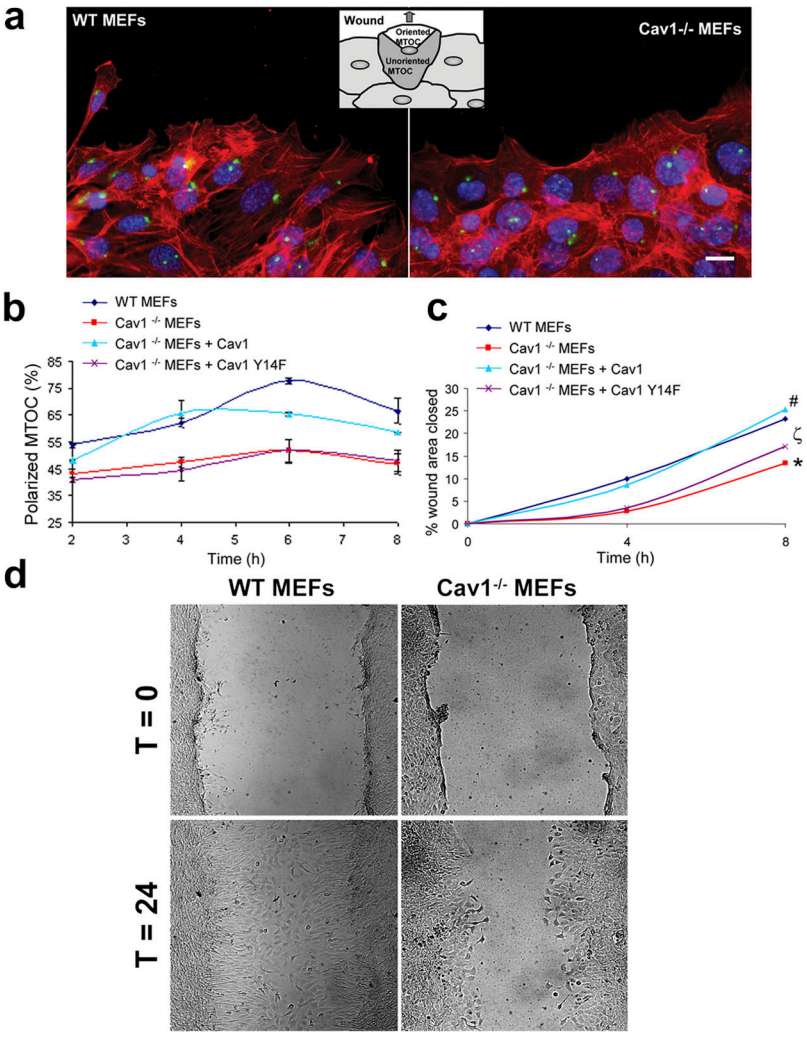

Figure 2. **Polarity is impaired in Cav1$^{-/-}$ MEFs.** (a) MEF monolayers were fixed 2, 4, 6, and 8 h after scratching and immunostained for DNA (blue), actin (red), and pericentrin (green), a marker for the MTOC. Representative wound-edge WT and Cav1$^{-/-}$ MEFs are shown. The criteria for MTOC polarization is explained in the diagram. Bar, 20 μm. (b) The percentage of cells in the front row showing reoriented MTOC was measured at the indicated times after wounding. For each time point, 150–300 cells were scored. Values represent means ± SEM of three independent experiments. (c) Graphical representation of wound closure in WT MEFs, Cav1$^{-/-}$ MEFs, and Cav1$^{-/-}$ MEFs reconstituted with caveolin-1 or caveolin-1 Y14F are shown. The percentage of closure was measured at 4 and 8 h after wounding. Error bars show SEM from six independent experiments. For 4 h, p values are as follows: *, P = 0.024 (Cav1$^{-/-}$ versus WT MEFs); $^{\#}$, P = 0.033 (Cav1$^{-/-}$ + Cav1 versus Cav1$^{-/-}$ MEFs); $^{\zeta}$, P = 0.039 (Cav1$^{-/-}$ + Cav1Y14F versus WT MEFs). For 8 h, p values are as follows: *, P = 0.020 (Cav1$^{-/-}$ versus WT MEFs); $^{\#}$, P = 0.042 (Cav1$^{-/-}$ + Cav1 versus Cav1$^{-/-}$ MEFs); $^{\zeta}$, P = 0.049 (Cav1$^{-/-}$ + Cav1Y14F versus WT MEFs). (d) WT and Cav1$^{-/-}$ MEF monolayers were scraped with a plastic pipette tip and photographed immediately (t = 0) or after 24 h (t = 24).

Published May 21, 2007

Caveolin-1 regulates GTP loading of Rho GTPases and their downstream biological consequences

Impaired polarization and defects in the stress fiber and FA pattern in Cav1$^{-/-}$ fibroblasts suggest alterations in the activity of the GTPases of the Rho family, as they are the principal regulators of these processes (Burridge and Wennerberg, 2004; Raftopoulou and Hall, 2004; Vicente-Manzanares et al., 2005; Pertz et al., 2006). To test this hypothesis, we performed pull-down assays to determine the level of activation of Rho, Rac, and Cdc42 in WT and Cav1$^{-/-}$ MEFs. We found that caveolin-deficient MEFs showed a notable decrease in basal Rho activity and a significant increase in Rac and Cdc42 activity (Fig. 3). To confirm these biochemical observations, we performed several assays designed to test biological consequences downstream of GTPases, namely, protrusion formation and lifetime of nascent adhesions at protruding areas. Time-lapse video recording of paxillin-GFP–expressing MEFs revealed that the lifetime of newly forming adhesions at protruding regions was twofold shorter in Cav1$^{-/-}$ MEFs compared with WT cells (Fig. 4 and Videos 1 and 2, available at http://www.jcb.org/cgi/content/full/jcb.200701006/DC1) and was rescued by caveolin-1 expression (Fig. 4). Increased adhesion turnover speed at cell protrusions in Cav1$^{-/-}$ MEFs is consistent with reduced Rho activity, which could be essential for the maturation of small focal complexes into FAs. In this regard, increased Rac and Cdc42 activity fits with the higher number of immature focal complexes observed in the Cav1$^{-/-}$ MEFs (Fig. 4 a, magnified areas). To test whether hyperactivation of Rac and Cdc42 has consequences in membrane protrusion, we performed time-lapse analysis of the protrusive–retractile activity at cell edges. Both protrusive and retractile activities were significantly higher in Cav1$^{-/-}$ MEFs (Fig. 5 and Videos 3 and 4). Careful observation

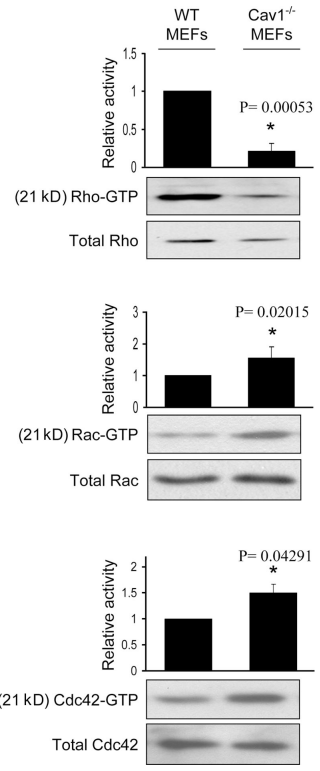

Figure 3. **Cav1$^{-/-}$ MEFs show alterations in the activity of Rho GTPases.** WT and Cav1$^{-/-}$ MEFs were lysed, and pull-down assays were performed as described in Materials and methods. Proteins bound to GST-PAK binding domain (for Rac and Cdc42) or GST-Rhotekin binding domain (for Rho) were separated by 13% SDS-PAGE, transferred to a polyvinylidene difluoride membrane, and immunoblotted with one of the following antibodies: anti-Rho, anti-Rac1, or anti-Cdc42. Representative Western blots of each GTPase are shown. The diagrams illustrate densitometric analysis of the relative activities of Rho, Rac, and Cdc42, normalized for whole cell lysates and expressed as a ratio to WT MEFs (means ± SEM of five to six independent experiments). *, Statistically significant versus WT MEFs.

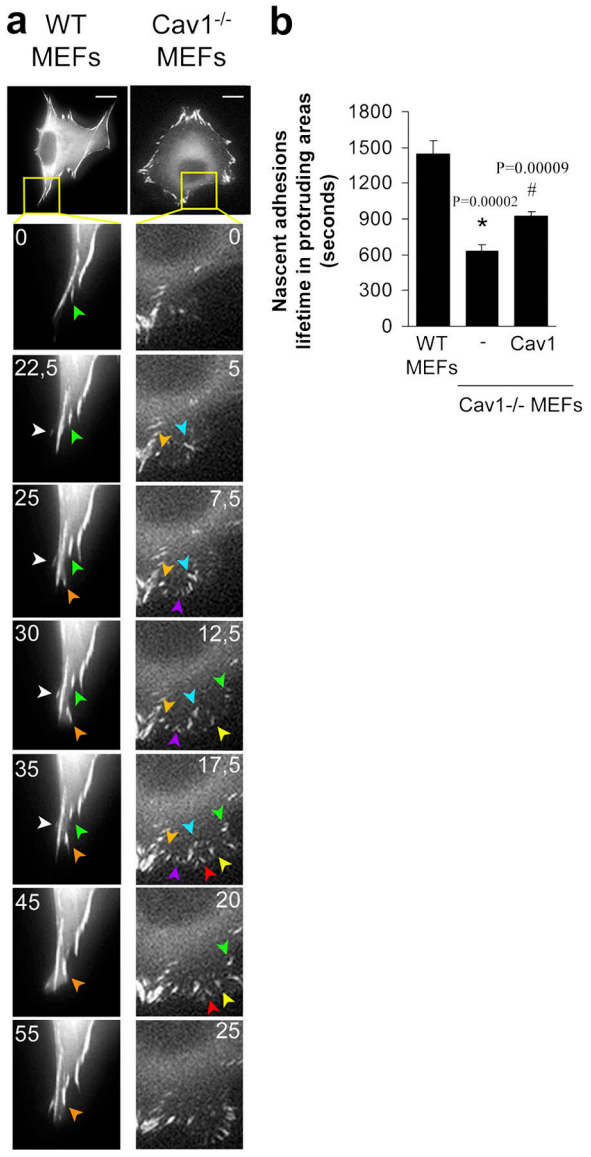

Figure 4. **Cells lacking caveolin-1 show accelerated turnover of nascent adhesions at protruding areas.** (a) Cells were transiently transfected with pEGFP-paxillin and plated on an Fn matrix, and turnover of newly forming adhesions in protruding areas was monitored by time-lapse video microscopy. Seven frames of two representative cells are shown. The lifetime of several adhesions was followed and pointed with colored arrowheads. Each color indicates a different adhesion. Bars, 20 μm. (b) The lifetimes of adhesions were determined in 16 WT cells (274 FAs), 15 Cav1$^{-/-}$ MEFs (376 FAs), and 10 Cav1$^{-/-}$ MEFs reconstituted with caveolin-1 (354 FAs). Values are means ± SEM. *, Statistically significant versus WT MEFs; #, statistically significant versus Cav1$^{-/-}$ MEFs.

Published May 21, 2007

of these videos revealed that protrusive activity in WT MEFs is highly directional, i.e., it only occurs in the direction of movement, whereas retraction occurs preferentially at the rear end. However, in Cav1$^{-/-}$ MEFs, protrusion and retraction is higher and occurs concomitantly throughout the cell perimeter (Fig. 5 and Videos 3 and 4). Quantification of the protrusive and retractile area showed a significant increase in Cav1$^{-/-}$ MEFs compared with WT MEFs (Fig. 5, b and c).

Altogether, these results indicated that changes in the activity of Rho GTPases could be responsible for the morphological defects observed in Cav1$^{-/-}$ fibroblasts. To test this hypothesis, we reconstituted the normal GTPase pattern of activity by expressing a constitutively active mutant of Rho (GFP-Rho G14V) or dominant-negative mutants of Rac (GFP-Rac T17N) or Cdc42 (GFP-Cdc42 T17N) in Cav1$^{-/-}$ fibroblasts. Expression of each individual construct was able to restore the WT elongated phenotype (Fig. S2, available at http://www.jcb.org/cgi/content/full/jcb.200701006/DC1). This result most likely reflects the fact that alteration of the proper reciprocal balance between Rho GTPases could account for the polarization defects of Cav1$^{-/-}$ cells.

Directional migration is impaired in cells lacking caveolin-1

A role for caveolin-1 in cell motility has been previously suggested, although contradictory effects have been reported. In an attempt to elucidate this issue, we performed several migration assays with Cav1$^{-/-}$ MEFs. As a first approach, we measured the velocity of random migration of these cells on a Fn matrix, using time-lapse microscopy. We found that Cav1$^{-/-}$ MEFs moved subtly faster compared with WT MEFs (Fig. 6, a and b). However, important differences were observed in the pattern of migration of Cav1$^{-/-}$ versus WT MEFs (Videos 5 and 6, available at http://www.jcb.org/cgi/content/full/jcb.200701006/DC1). WT cells showed an intrinsic directionality or persistency of migration, i.e., they tend to migrate in the same direction for a sustained period of time without turning even in the absence of a chemotactic gradient, whereas Cav1$^{-/-}$ MEFs completely lost directionality. This observation was confirmed by measuring the trajectory of each individual cell during a 10-h migration period by tracking its centroid from the time-lapse video. To clearly visualize the differences, cell movement paths were reproduced on composite panels (Fig. 6 c). Interestingly, we found that Cav1$^{-/-}$ MEFs displayed much shorter net translocation (the shortest linear distance from the starting point to the end point of the time-lapse recording) than the WT cells, which showed longer paths and migrated on a straighter way. To quantify these differences, we measured the directional persistence of the cells as estimated by the index of directionality (ID; i.e., the ratio of the net distance divided by the total distance traveled by the cell). The Cav1$^{-/-}$ MEFs showed a significant reduction in the ID (Fig. 6 d) that was restored by caveolin-1 reexpression (Fig. 6, c and d; and Video 7). These results show that caveolin-1 contributes to persistent migration, i.e., the cell's internal sense of directionality. To explore directional migration stimulated by external stimuli, we performed wound-healing and chemotaxis assays. Both wound closure (Fig. 2, c and d; and Videos 8 and 9) and the chemotactic response in a transwell assay (Fig. 6 e) were hampered in caveolin-1–deficient MEFs, and reconstituting caveolin-1 expression rescued both responses (Video 10). Collectively, these data demonstrate that caveolin is required in fibroblasts for persistency of migration in the absence of an external chemotactic cue and for directional migration in the presence of an external stimulus, whereas it slightly slows down the velocity of random migration.

Src and p190RhoGAP are involved in the loss of polarity of the Cav1$^{-/-}$ cells

Caveolin-1 is a substrate for nonreceptor tyrosine kinases, including Src. In fact, caveolin-1 was first described as the major substrate for Src in v-src transformed cell lines (Glenney and Zokas, 1989). Furthermore, it has been described that caveolin phosphorylated on Tyr 14 (pY14-Cav1) can inhibit Src through the recruitment of C-terminal Src kinase (Csk; Cao et al., 2002; Radel and Rizzo, 2005). Thus, we hypothesized that in the

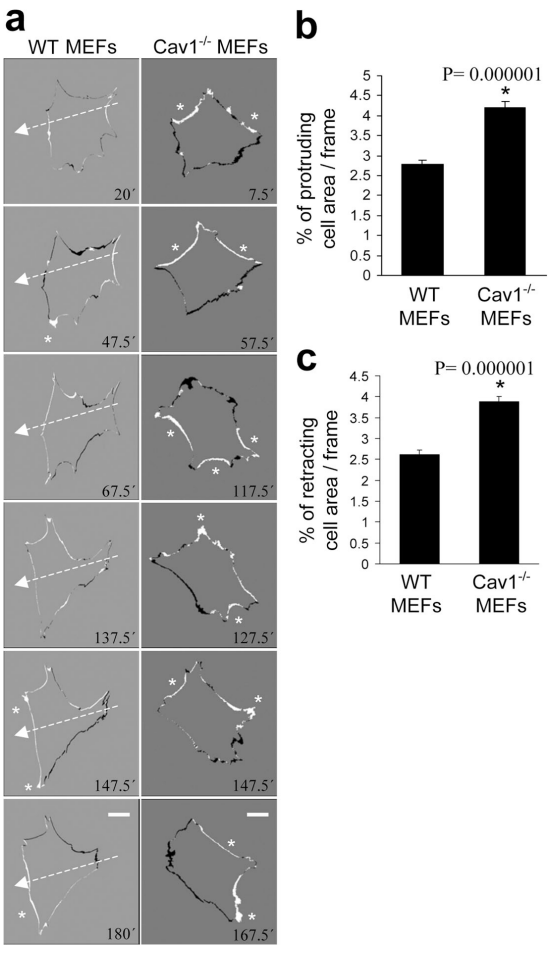

Figure 5. **Cells lacking caveolin-1 show enhanced protrusive activity.** (a) The time-lapse paxillin videos (Fig. 4) were used to calculate cell protrusion as described in Materials and methods. Six subtracted consecutive frames of two representative cells are shown. White areas are the protruded edges, and black areas are retracted edges between two consecutive frames. White arrows indicate the direction of cell movement in the WT cell, and asterisks point to large protrusive areas. Note that Cav1$^{-/-}$ MEFs did not persistently move in a defined direction. Areas of protrusions (b) and retractions (c) were meas ured and plotted. Data shown are means ± SD. *, Statistically significant versus WT MEFs. Bars, 20 μm.

Published May 21, 2007

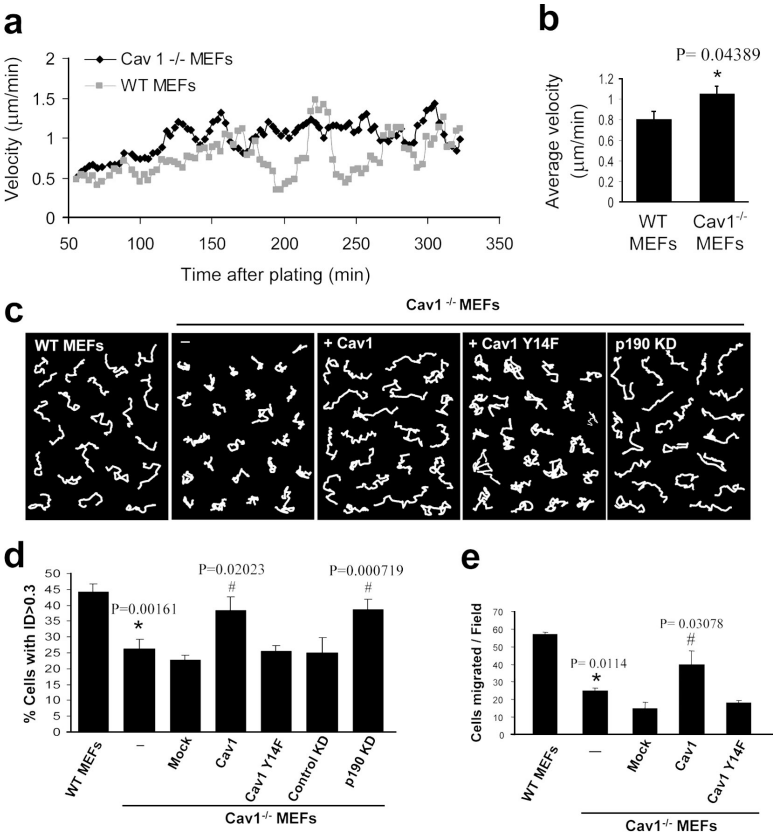

Figure 6. **Directional migration is impaired in Cav1$^{-/-}$ MEFs and can be rescued by WT Cav1 and p190RhoGAP knockdown, but not by Cav1Y14F.** WT and Cav1$^{-/-}$ MEFs plated on Fn were recorded in random migration by time-lapse video microscopy during a 10-h period (8-min frame interval). (a) Instantaneous velocities of 580–600 cells of each type were quantified and plotted over time on Fn. Cell densities of both populations were equivalent (not depicted). (b) Histograms represent the mean velocities over the 90–330-min period, at which time steady-state velocities were reached. (c) White lines show representative migration tracks of the cell lines indicated at the top of each panel. Composite migration figures were created by coping randomly selected individual migration paths and combining them into a single figure to avoid empty spaces (Pankov et al., 2005). (d) The ID was quantified with Matlab and MetaMorph software. Histograms display the percentage of cells with ID > 0.3 in each cell line. This value (0.3) was the highest mean ID displayed in all experimental conditions tested, and therefore the percentage of cells with ID > 0.3 represents highly directional migratory cells. Data represent means ± SEM based on six independent experiments. n = 300–500 cells of each line. (e) Transwell filters coated with Fn were used to measure the chemotactic response of WT MEFs, Cav1$^{-/-}$ MEFs, and Cav1$^{-/-}$ MEFs reconstituted with caveolin-1 or caveolin-1 Y14F using serum as a stimulus. Cells that had migrated during 4 h to the lower surface of the filters were counted in five random fields. Means ± SD from four independent experiments are shown. *, Statistically significant versus WT MEFs; #, statistically significant versus Cav1$^{-/-}$ MEFs.

absence of caveolin-1, Src activity could be affected. We evaluated the Tyr 418 phosphorylation state of Src in Cav1$^{-/-}$ MEFs and found an increase in the basal activation of Src (Fig. 7 a; quantified in Fig. 7 b), accompanied by a reduction in the abundance of this protein (Fig. 7, a and c), consistent with the reported increased degradation of active versus inactive Src (Hakak and Martin, 1999). Increased Src activity in Cav1$^{-/-}$ MEFs suggested that Src could be involved in the morphological changes observed in the absence of caveolin-1. To test this hypothesis, we blocked Src activation by treating the Cav1$^{-/-}$ MEFs with two inhibitors of Src family kinases, PP2 and SU6656. Interestingly enough, Src inhibition restored the morphological phenotype of the WT MEFs (Fig. 7, d and e; and Fig. S4). Because Src regulates caveolin-1 through phosphorylation of Tyr 14, one requirement of our hypothesis is that expression of a nonphosphorylable mutant of caveolin-1 in Cav1$^{-/-}$ MEFs should not restore the normal phenotype. Accordingly, cells stably transfected with the Y14F caveolin-1 mutant (Fig. 1 d) did not restore the cell morphological changes (Fig. 7 g), MTOC polarization (Fig. 2 b), wound closure (Fig. 2 c), directionally persistent migration (Fig. 6, c and d), or the chemotactic response (Fig. 6 e), which were restored by WT Cav1 in all cases. These results highlight the importance of caveolin-1 Tyr 14 phosphorylation by Src in the polarization and directed motility of mouse fibroblasts.

Several links have been reported between the activity of Src kinase and Rho GTPases. Thus, Src is involved in activation of Rac (Servitja et al., 2003; Kawakatsu et al., 2005) and Cdc42 (Miyamoto et al., 2003; Tu et al., 2003; Fukuyama et al., 2005) and can inhibit Rho through activation of p190RhoGAP (Arthur et al., 2000; Brouns et al., 2001; Meng et al., 2004). Therefore, increased Src activity could explain the reduction in Rho GTP levels observed in Cav1$^{-/-}$ fibroblasts through activation of p190RhoGAP. Both total protein and tyrosine phosphorylated p190RhoGAP levels are mildly elevated in Cav1$^{-/-}$ cells (Fig. S5, available at http://www.jcb.org/cgi/content/full/jcb.200701006/DC1), supporting this notion. To test this hypothesis, we expressed a dominant-negative mutant of p190RhoGAP in Cav1$^{-/-}$ fibroblasts and measured the EF. Importantly, GFP-p190 R1283A–expressing Cav1$^{-/-}$ fibroblasts showed an elongated shape (Fig. S3). Moreover, knocking down p190RhoGAP expression using RNA interference (Fig. 7 f) led to a recovery of the morphological changes (Fig. 7, d and e; and Fig. S4) and persistent migration defects (Fig. 6 c; quantified in Fig. 6 d). Both Src inhibition and RhoGAP knockdown individually were able to rescue the various phenotypes to the levels achieved in WT cells, and they did not display an additive effect when combining both treatments (Fig. 7, d and e; and Fig. S4). These results suggest that a linear pathway of Src and p190RhoGAP activities drives Rho down-regulation in cells lacking caveolin-1. In this regard, expression of WT caveolin-1, but not the Y14F caveolin-1 mutant, restored Rho GTP loading in Cav1$^{-/-}$ MEFs (Fig. 7, h and i). These findings suggest an important role of caveolin-1 and Src in the establishment of cell polarity by regulating the activity of Rho. Our results support a model in which, in the absence of caveolin-1 expression, Src activity may become insensitive to Csk modulation; increased Src could inactivate Rho in a p190RhoGAP-dependent manner, resulting in profound defects in cell polarization and directed migration.

Published May 21, 2007

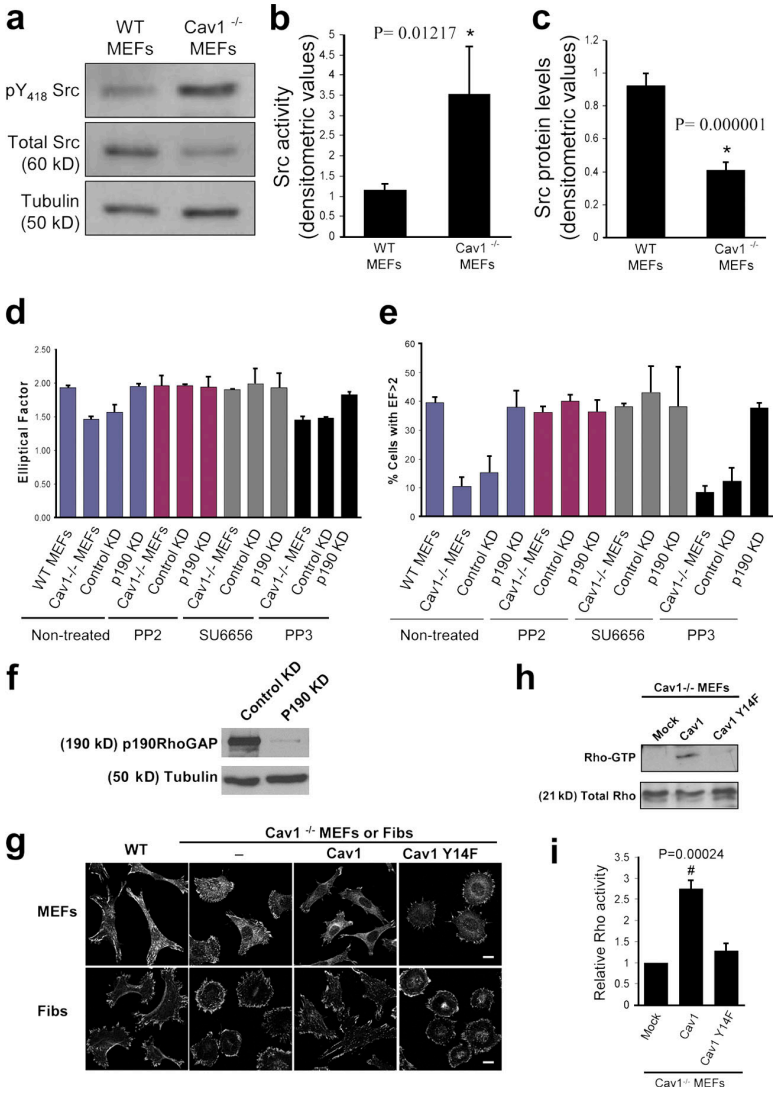

Figure 7. **Altered phenotype of Cav1$^{-/-}$ fibroblasts is dependent on Src and p190RhoGAP.** (a) Activated and total Src were assayed by Western blotting with anti-Src(pY418) phosphospecific antibody and anti-Src pan antibody, respectively. Each of the illustrated blots is representative of five experiments. (b) Src activity was determined densitometrically and expressed as the Src(pY418)/Src ratio. (c) Src protein levels were normalized to tubulin levels in each sample. Values depict means ± SEM of five independent experiments. (d) Both Src inhibition and p190RhoGAP knockdown in Cav1$^{-/-}$ MEFs restore the WT morphology pattern. EF was calculated for Cav1$^{-/-}$ MEFs treated with two different Src inhibitors, PP2 and SU6656. PP3 was used as a negative control. Data indicate means ± SEM (n = 3). (e) Percentages of cells with EF >2 are shown for each population (n >100 cells per condition). Values represent means ± SEM from three independent experiments. (f) Cav1$^{-/-}$ MEFs were infected with retroviruses encoding for control (control KD) or p190RhoGAP shRNA (p190 KD). Positive cells were sorted, and knock down was confirmed by a Western blot against p190RhoGAP. As a loading control, anti-tubulin immunoblot is shown. 95% reduction in p190RhoGAP levels was obtained. (g) Cells were plated on Fn-coated plates for 4 h, fixed, and stained with anti-paxillin antibodies. Representative images of each cell line are shown. Fibs, thymus fibroblasts. Bars, 20 μm. (h) Cav1$^{-/-}$ MEFs reconstituted with empty vector (mock), caveolin-1, or caveolin-1 Y14F were lysed, and pull-down assays were performed as described in Materials and methods. Proteins bound to GST-Rhotekin binding domain (top) and whole cell lysates (bottom) were separated on a 13% SDS-PAGE, transferred to a polyvinylidene difluoride membrane, and immunoblotted with anti-Rho antibodies. (i) The histograms illustrate densitometric analysis of the relative activity of Rho normalized for whole cell lysates and relative to control cells. Means ± SEM of six independent experiments are shown. #, Statistically significant versus Cav1$^{-/-}$ MEFs transfected with the empty vector.

Impaired skin wound healing in caveolin-1–deficient mice

To explore whether the differences in the migratory behavior observed ex vivo have any correspondence in vivo, we performed wound-healing experiments in the skin of 11-wk-old WT and Cav1$^{-/-}$ mice. Wound healing is a complex process involving growth factors, ECM, and epidermal and mesenchymal cells undergoing directional migration, proliferation, and differentiation events (Singer and Clark, 1999). Two 3.5-mm-diameter circular punch biopsies were performed on the back skin of five WT and five Cav1$^{-/-}$ mice. The rate of wound healing was monitored as the percentage of the initial wound area left open with time after the punch was made. Cav1$^{-/-}$ mice showed a significantly slower wound healing rate compared with WT littermates (Fig. 8 a). As examples, Fig. 8 b shows representative images of WT and Cav1$^{-/-}$ wounds 1 and 7 d after the wounds were made. These results indicate that the skin of Cav1$^{-/-}$ mice has an impairment in wound healing. Provided the hyperproliferative phenotype of Cav1$^{-/-}$ mice (Drab et al., 2001; Razani et al., 2001), these in vivo findings support our ex vivo observations that caveolin-1 is required for directional migration.

Discussion

Caveolin-1 is one of the numerous intracellular signaling molecules that have been implicated in cell migration. However, there is no consensus on its role in controlling cell motility, as both positive (Galvez et al., 2004; Ge and Pachter, 2004; Podar et al., 2004) and negative (Zhang et al., 2000; Gonzalez et al., 2004) regulatory effects have been reported. Technical or cell type specificity issues most likely account for this discrepancy. However, provided the relevance of both caveolin-1 and cell migration in both physiology and many pathological conditions, it seems important to further investigate this controversy. In this study, we analyze fibroblasts prepared from two types of Cav1$^{-/-}$ mouse (Razani et al., 2001; Valasek et al., 2005) in a variety of polarization and migration assays, including random and directional migration approaches. We have obtained evidence for the requirement of caveolin-1 for the establishment of a polarized and elongated morphology, internal persistency of migration, and externally stimulated directional migration. We show that caveolin-1 regulates polarity and directional migration by affecting the activation patterns of Src and Rho GTPases.

Published May 21, 2007

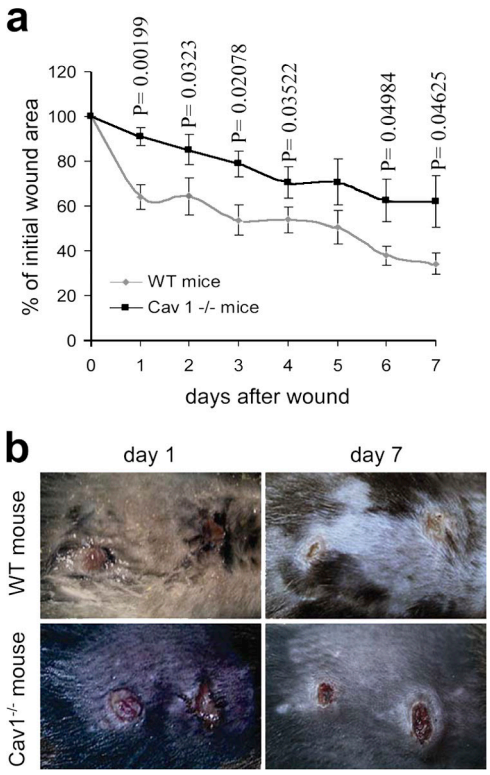

Figure 8. **Wound healing in skin of WT and Cav1$^{-/-}$ mice.** Two wounds were created per mouse in five Cav1$^{-/-}$ mice and five WT mice (n = 10). (a) The graph represents the percentage of initial wound area left at the indicated days after the punch was made (mean ± SEM). Statistical analysis shows that the healing rate is significantly different between genotypes 1–4, 6, and 7 d after wound creation (p-values). (b) Representative images of wounds 1 and 7 d after wound creation are shown.

Our results suggest a model in which the modulation of Src activation by the caveolin-1–Csk module (Cao et al., 2002; Radel and Rizzo, 2005) is crucial for the establishment of cell polarity and directional migration. In caveolin-1–deficient cells, Src activity is constitutively high, leading to a p190RhoGAP-dependent decrease in the levels of GTP-loaded Rho and subsequent defects in the arrangement of the actin cytoskeleton.

The first and evident feature we observed in the Cav1$^{-/-}$ fibroblasts is a profound change in their morphology and in the actin cytoskeleton architecture. Most of them were rounded and showed stress fibers localized in the cell periphery, creating concentric cortical actin rings. This phenotype suggested alterations in the activity of the GTPases of the Rho family, as they are the principal regulators of polarity and cytoskeletal rearrangements (Burridge and Wennerberg, 2004; Raftopoulou and Hall, 2004; Vicente-Manzanares et al., 2005; Pertz et al., 2006). We found that Cav1$^{-/-}$ fibroblasts showed a dramatic decrease in basal Rho activity and a significant increase in Cdc42 and Rac activity, the latter consistent with the reported data for Rac activity upon caveolin-1 silencing (Gonzalez et al., 2004). On the other hand, Cav1$^{-/-}$ fibroblasts presented shorter lifetime of nascent adhesions at protrusive areas, compared with the control cells. This is consistent with the low levels of Rho GTP loading, as adhesion turnover inversely correlates with Rho activity (Ren et al., 2000). In addition, these adhesive complexes were smaller and more abundant in Cav1$^{-/-}$ than in WT fibroblasts. This fact indicates a possible blockage in the maturation of these structures, which is also dependent on Rho (Rottner et al., 1999; Geiger and Bershadsky, 2001). The increase in Rac and Cdc42 GTP levels also supports this phenotype, as both GTPases are involved in the creation of new substrate contacts and recruitment of cytoskeletal and signaling proteins into nascent small focal complexes (Rottner et al., 1999; Vicente-Manzanares et al., 2005). Likewise, we found an enhanced, nondirectional protrusive activity in the whole periphery of caveolin-1–deficient cells, in agreement with the altered pattern of activity of Rho GTPases. In fact, both Rho inactivation (Arthur and Burridge, 2001) and Rac activation promote membrane protrusion (Machesky and Hall, 1997; Raftopoulou and Hall, 2004), and there is evidence of a mutual antagonism between both GTPases (Rottner et al., 1999; Sander et al., 1999; Nimnual et al., 2003; Xu et al., 2003; Burridge and Wennerberg, 2004). Interestingly, the use of a fluorescence resonance energy transfer biosensor to measure local activation of Rho has recently established that Rho is active in a sharp band immediately adjacent to the leading edge of migrating cells, both randomly and in a wounded monolayer (Kurokawa and Matsuda, 2005; Pertz et al., 2006). This suggests that Rho is also required for directional migration, and not only for cell contraction, as it was previously established. The dramatic decrease of Rho activity in caveolin-1–deficient cells together with the lack of directionality in these cells is consistent with these reports. The fact that each individual Rho GTPase mutant (active Rho or inactive Rac/Cdc42) restore the normal polarized phenotype is intriguing. The pattern of activity of all three Rho GTPases is altered in caveolin-deficient cells, which complicates the interpretation of this result. It could be explained by the mutual inhibition between the frontness (Rac/Cdc42 dependent) and backness (Rho dependent) pathways (Li et al., 2003; Meili and Firtel, 2003; Xu et al., 2003). Therefore, this result does not necessarily imply that alterations in the GTP loading of each GTPase play a direct role in the phenotype observed in Cav1$^{-/-}$ fibroblasts, as this could be an indirect effect, through a negative feedback on the opposing pole of the cell. For Rac, apart from increased GTP loading, enhanced plasma membrane targeting in caveolin-1–deficient cells (Del Pozo et al., 2005) could be partially responsible for the phenotype observed. In any case, alteration of the normal reciprocal balance between Rho GTPases most likely contributes to the aberrant cellular morphology and migratory behavior of Cav1$^{-/-}$ cells.

Consistent with the morphological phenotype, Cav1$^{-/-}$ fibroblasts show a remarkable defect in directional migration, both externally stimulated and internally persistent. Persistence is the intrinsic propensity of the cells to continue migrating in the same direction in the absence of exogenous stimuli (Huttenlocher, 2005). Recently, Pankov et al. (2005) showed that high Rac activity renders a random migration pattern, whereas decreasing Rac activity switches cell migration from random to directionally persistent. Consistently, we found a mild but significant increase in the velocity of random migration and a dramatic switch toward random migration in Cav1$^{-/-}$ fibroblasts, concomitant with increased Rac GTP levels. Thus, increased Rac activity and/or enhanced Rac membrane targeting

Published May 21, 2007

in caveolin-1–deficient cells (Del Pozo et al., 2005) would render nonpolarized increased protrusive activity throughout the whole cell perimeter and, consequently, loss of directionally persistent cell migration. Previous reports where caveolin-1 expression inhibited cell migration (Zhang et al., 2000; Gonzalez et al., 2004; Hassan et al., 2006) fit with our result that Cav1$^{-/-}$ cells migrate slightly faster in the absence of an external chemotactic cue. Therefore, previous contradictory results could be reconciled by a detailed analysis of random versus directional migration in caveolin-1–deficient cells. In other cases, divergent results can be ascribed to technical or cell-specific issues. In this regard, a recent report showed that caveolin-1–deficient aortic smooth muscle cells are slightly more migratory than the control cells (Hassan et al., 2006). However, these cells express caveolin-3, which could compensate the absence of caveolin-1. Moreover, these cells were isolated from Ink4a$^{-/-}$ mice, which show increased proliferation (Hassan et al., 2006), which could influence the observed results.

The phenotypic deficiencies reported in Cav1$^{-/-}$ fibroblasts are dependent on caveolin-1, as restoring its expression rescues the WT phenotype. Importantly, this recovery is dependent on caveolin-1 Tyr 14, which is the substrate for Src phosphorylation (Glenney and Zokas, 1989). This phosphorylation is important for fine-tuning of Src activation, as pY14-Cav1 binds to and activates Csk, which phosphorylates inhibitory Tyr 527, resulting in Src inactivation, closing a negative feedback loop (Cao et al., 2002; Radel and Rizzo, 2005). These results predict that in the absence of pY14-Cav1, Src should be insensitive to modulation by Csk. Accordingly, we find increased Src activation in Cav1$^{-/-}$ fibroblasts, and when these cells were reconstituted with a Src-insensitive Y14F caveolin-1 mutant, the normal phenotype was not restored. Increased Src activation was accompanied by a reduction in the protein levels, consistent with previous reports that Src activation leads to increased polyubiquitination and proteasome-dependent degradation (Hakak and Martin, 1999). In spite of protein reduction levels, increased Src activation is functionally relevant because pharmacological inhibition of Src in Cav1$^{-/-}$ fibroblasts restored the normal phenotype.

Mechanistically, we have found that alterations in the signaling of both Src kinase and Rho GTPases are responsible for the aberrant morphology and migratory pattern of Cav1$^{-/-}$ cells. Our results and previous reports allow us to envisage a model in which caveolin-1 influences signaling of Rho GTPases through activated Src. Src regulates the activity of the three major Rho GTPases studied here. It can activate Cdc42 through many pathways, including the exchange factors FRG (Miyamoto et al., 2003), Vav2 (Tu et al., 2003), and C3G (in collaboration with Crk, Rap1, and FRG; Fukuyama et al., 2005). It activates Rac through the exchange factors Dock180 (in collaboration with p130Cas and Crk; DeMali et al., 2003), Tiam1, Vav2 (Servitja et al., 2003), and FRG (through Cdc42 and Vav2; Kawakatsu et al., 2005). However, Src inhibits Rho activity through activation of p190RhoGAP (Arthur et al., 2000; Brouns et al., 2001; Meng et al., 2004). We present evidence that p190RhoGAP is involved in caveolin-mediated alterations of the cell polarity, allowing us to propose this model.

The ex vivo migratory defects reported here are most likely related to the in vivo impaired angiogenic response displayed by Cav1$^{-/-}$ mice (Woodman et al., 2003; Sonveaux et al., 2004) and could account for it. Angiogenesis is a complex phenomenon involving both migration and proliferation of endothelial cells (Woodman et al., 2003). In spite of increased cellular proliferation, Matrigel plugs implanted in Cav1$^{-/-}$ mice showed reduced blood vessel formation (Woodman et al., 2003), suggesting that decreased migration is most likely responsible for the angiogenic defects. In good agreement, knocking down caveolin-1 expression diminishes the chemotactic response in endothelial cells in vitro (Galvez et al., 2004). We also report here an impaired in vivo wound healing in Cav1$^{-/-}$ mice. Wound healing is also a complex process that depends on directional migration, proliferation, and differentiation of epidermal and mesenchymal cells (Singer and Clark, 1999). Because enhanced cell proliferation of Cav1$^{-/-}$ mice (Drab et al., 2001; Razani et al., 2001) would favor the wound-healing process, our results support the notion that decreased directional migration accounts for decreased wound healing observed in vivo. However, caveolin-1 appears to be dispensable for normal embryonic development, as Cav1$^{-/-}$ mice are viable (Drab et al., 2001; Razani et al., 2001). Although embryonic development of these animals has not been studied in detail, most likely other signaling pathways involved in the complex migratory process (Ridley et al., 2003; Vicente-Manzanares et al., 2005) are compensating for caveolin-1 absence. Caveolin-deficient animals display a wide range of phenotypes (Le Lay and Kurzchalia, 2005), and it seems feasible that some of them might be related to the migratory deficiencies reported here. Elucidating such phenotypes is an interesting goal for future work.

Materials and methods

Handling of mice

Caveolin-1–deficient mice strain Cav-1^{tm1Mls}/J and their WT littermates were obtained from The Jackson Laboratory. Mice were housed and maintained in a barrier facility at our institute (Centro Nacional de Investigaciones Cardiovasculares, Madrid, Spain), which approved the animal protocols. Pathogen-free procedures are used in all mouse rooms. Quarterly health-monitoring reports have been negative for all pathogens in accordance with Federation of European Laboratory Animal Science Associations recommendations. Mice were kept on a 12:12-h light–dark cycle, with ad libitum access to food and water.

Cell culture

MEFs (Razani et al., 2001) and thymus fibroblasts (Valasek et al., 2005) from Cav1$^{-/-}$ and Cav1$^{+/+}$ littermate mice have been used throughout this study. M.P. Lisanti (Thomas Jefferson University, Philadelphia, PA) and R.G.W. Anderson (University of Texas Southwestern Medical Center, Dallas, TX) provided MEFs and thymus fibroblasts from Cav$^{-/-}$ and Cav$^{+/+}$ littermate mice, respectively. All experiments were performed with both cell types, except from the MTOC polarization assay, Rho GTPase pull downs, and FA lifetime estimations, which were performed only with the MEFs. Cells were maintained in culture in DME supplemented with 10% FBS, 100 U/ml penicillin, and 100 μg/ml streptomycin.

DNA plasmids and constructs

Plasmids encoding pEGFP-p190RhoGAP R1283A (Noren et al., 2003); pEGFP-paxillin (Nishiya et al., 2005); and GFP-tagged Rac T17N, Cdc42 T17N, and Rho G14V (del Pozo et al., 1999) were previously described. K. Burridge (University of North Carolina at Chapel Hill, Chapel Hill, NC) provided GFP-p190 R1283A. C-terminal Flag-tagged mouse caveolin-1 was cut with BamH1–EcoRI, blunt-ended, and ligated to blunt-ended MIGR1

Published May 21, 2007

EcoRI, a bicistronic, GFP-expressing retroviral vector (Pear et al., 1998). C-terminal Flag tag caveolin-1 Y14F was cut with BglII–BamH1 and ligated to BglII site in MIGR1.

Generation of stable cell lines by retroviral infection
NIH 3T3 or 293T/17 cells were transfected (using Lipofectamine 2000 or calcium phosphate method) with MIGR1, MIGR1–caveolin-1 or MIGR1–caveolin-1Y14F and packaging plasmid pSVψ2. 48 h later, supernatants were filtered and added to Cav1$^{-/-}$ MEFs in DME plus 10% FBS containing 4 μg/ml polybrene. 48 h later, GFP-positive cells were sorted using a cell sorter (DakoCytomation). Levels of caveolin-1 and caveolin-1 Y14F were similar to endogenous caveolin-1 in MEFs (Fig. 1 d).

RNA interference–mediated knock down of p190RhoGAP
Mouse p190RhoGAP (available from GenBank/EMBL/DDBJ under accession no. NM_172739) targeting sequence (nucleotides 2935–2953, 5′-gttatggacgcaacattaa-3′) and control, nontargeting sequence (5′-gcgcgctttgtaggattcg-3′) were cloned into short hairpin RNA (shRNA) vector pSuper.Retro.Neo+GFP (Oligoengine) to generate pSuperRetroGFP-p190-2935 and pSuperRetroGFP-Control vectors. Retroviral supernatants were generated by transfecting 293T/17 cells with each shRNA and pSVψ2 vector using Fugene 6 (Roche) transfection reagent. Cav-1$^{-/-}$ MEFs were infected with retroviral supernatants as previously indicated, and high GFP-expressing cells were sorted (∼15% of the cell population).

Antibodies and reagents
mAb against p190RhoGAP was purchased from BD Biosciences. pAb against Cdc42 and mAb against Rho were purchased from Santa Cruz Biotechnology, Inc. Anti-Rac, anti-Src and anti-phosphotyrosine (4G10) mAbs were obtained from Upstate Biotechnology, mAb for vinculin was obtained from Sigma-Aldrich, and anti-Src(pY418) phosphospecific pAb was purchased from Biosource International. Anti-paxillin mAb was purchased from Invitrogen. Rhodamine phalloidin and wheat germ agglutinin labeled with tetramethyl rhodamine were purchased from Invitrogen. Alexa 594 and FITC-conjugated antibody and peroxidase-conjugated goat anti–rabbit and anti–mouse IgG were obtained from Jackson ImmunoResearch Laboratories. Src kinase inhibitors SU6656 and PP2, as well as PP3 control, were obtained from Calbiochem. Fn was purified from human plasma as described previously (del Pozo et al., 2000).

Fluorescence microscopy
Cells were attached to glass coverslips precoated with 5 μg/ml Fn for different times. Cells were fixed with 2% formaldehyde-PBS for 20 min, permeabilized in 0.2% Triton X-100 in PBS for 10 min, and blocked with 10% normal goat serum before staining. Anti-vinculin/paxillin antibodies followed by FITC/Alexa594-conjugated anti-IgG were used to stain FAs. Actin cytoskeleton was stained with rhodamine phalloidin. For polarity determination, membrane of fixed cells was stained with 10 μg/ml wheat germ agglutinin for 30 min at RT. Images were acquired using a confocal microscope (Radiance 2100; Bio-Rad Laboratories, Inc.). Then, cells were outlined using the Kirsch edge detection algorithm, which is included in MetaMorph software (Universal Imaging Corp.). Outlines were checked and corrected by hand if necessary. Using MetaMorph's integrated morphometry analysis function, we determined the EF (length/breadth) of cells as a measure of elongation.

Chemotaxis assays
Transwell cell culture chambers containing polycarbonate membrane with 8-μm pore size (Corning Costar Corp.) were coated with 5 μg/ml Fn. Cells were starved for 24 h before experiments. After trypsinization and dilution, 15,000 cells in DME plus 0.2% BSA were added to the top Transwell chamber. The bottom compartment was filled with 500 μl DME plus 10% FBS, and the assembly was incubated at 37°C for 4 h, to allow cell migration. In the negative controls, bottom chambers were filled with DME plus 0.2% BSA. After incubation, the membranes were washed with PBS, and cells were fixed in 2% formaldehyde and stained with Hoechst 33342 (Sigma-Aldrich) according to the manufacturer's protocols. Cells that did not migrate were gently removed from the top surface, and cells that had migrated to the bottom of the membrane were counted in five random fields using a fluorescence microscope (Axiovert 200 M SP LSM5; Carl Zeiss MicroImaging, Inc.).

Time-lapse video microscopy and FA lifetime analysis
Cells were transiently transfected with pEGFP-paxillin 2 d before the experiment and were plated on a chambered coverglass (eight chambers; Lab-Tek) coated with 5 μg/ml Fn. After 45 min, chambers were filled with Optimem (Invitrogen) supplemented with 10% FBS, sealed using vacuum grease and a glass plate, and transferred to a microscope heated to 37°C. Image series of FA dynamics were acquired using a 60× 1.4 NA Plan Apo objective lens on an inverted microscope (Eclipse TE300; Nikon) heated with an airstream incubator (Nevtek) to 37°C. The microscope was equipped with a robotic stage with linear position feedback encoders on the x, y, and z axes (MS-2000; Applied Scientific Instruments) to allow image series to be collected at different stage positions over time. Images were captured using an cooled charge-coupled device camera (Orca II; Hamamatsu). Fluorescent and phase-contrast images were taken in rapid succession at multiple positions, evenly distributed over the chambers to exclude differences due to experimental variation, at 2.5-min intervals for 2.5 h. Phase-contrast image series of cell migratory behavior were collected on a similar microscope system, except using a 20× 0.5 NA Plan objective lens and a 0.5 NA extra-long working distance condenser, and were captured with a 10-bit chilled charge-coupled device camera (Orca 285; Hamamatsu). For image processing and analyses, we used MetaMorph software. Individual FAs were clearly distinguishable in the GFP-paxillin time-lapse image series. The time of formation and disappearance of the nascent adhesions from protruding areas of different cell types were monitored by eye and double-blind method. From the noted times of appearance and disappearance, the lifetimes of nascent adhesions in WT versus Cav1$^{-/-}$ cells were determined, averaged, and plotted, with the error bars indicating the SEM (Videos 1 and 2). To determine cell trajectories in phase-contrast time-lapse image series (cells filmed at 8-min intervals for 10 h), the centroids of the cell nuclei were followed (Videos 5–7). To automate this and allow the unbiased analysis of many cells in multiple time lapses, a program was written in Matlab (Mathworks; de Rooij et al., 2005), which segments images based on pixel intensity and determines the presence of nuclei based on phase density, size, and shape. Nuclei are then linked in consecutive frames using a neural network algorithm, and cells tracked for less than five consecutive frames are automatically discarded. Detection fidelity in our experiments was usually >90%, which was confirmed by eye for each individual time lapse. To prevent erratic conclusions because of false results generated by this automated analysis, a smaller number of random cells from several videos was tracked using the track objects function in MetaMorph, leading to the same results.

Protrusion–retraction analysis
Fluorescence time-lapse images of GFP-paxillin were used to outline cells by thresholding for pixels with high intensity. Areas covered by cells in consecutive images in the time series were subtracted to determine the percentage change of the total cell area contributing to protrusion or retraction occurring in the 2.5 min elapsed between the two images (Videos 3 and 4). Plotted are means of protrusion over the first 1.5 h of imaging from six different WT and seven different Cav1$^{-/-}$ cells.

In vitro wound-healing assay and determination of MTOC polarization
Cells were grown to confluence on coverglass chambers. Confluent monolayers were scraped with a 0.1–2 μl pipette tip. Wound closure was monitored by time-lapse video microscopy. Images were taken at 45-min intervals for 48 h (Videos 8–10). For MTOC polarization assay, cells were seeded on coverslips, and wounded monolayers were fixed 2, 4, 6, and 8 h after scraping. MTOC were localized by immunolabeling using anti-pericentrin antibodies. Only the first row of the wound edge was measured. Cells in which MTOC was contained by the quadrant facing the wound were scored positive (Fig. 2 a, diagram).

Wound-healing experiments in vivo
Two full-thickness punch biopsies extending through the epidermis and dermis (punch diameter 3.5 mm) were performed on the back of five WT and five Cav1$^{-/-}$ mice (11 wk of age) after depilation. Mice were anesthetized before wound creation. The wound-healing rate was calculated as the percentage of initial wound area with time. After capturing the images with a digital camera (DFC490; Leica), we determined the area of the wound with image analysis software (Leica IM50 Image Manager).

Pull-down assays and Western blot analysis
Rho, Rac, and Cdc42 activity were determined by pull-down assays as described before (del Pozo et al., 2000; Ren et al., 2000). Src activity was assayed by Western blotting.

Immunoprecipitation of p190RhoGAP
Low-density WT and Cav1$^{-/-}$ MEFs were lysed in RIPA buffer (10 mM Tris-HCl, pH 7.2, 1% Triton X-100, 0.5% sodium deoxycholate, 0.1% sodium dodecyl sulfate, 150 mM NaCl, 5 mM EDTA, and 3 mM EGTA) with phosphatase inhibitors (10 mM $Na_4P_2O_7$, 1 mM Na_3VO_4, 30 mM NaF, and 3 mM

β-glycerophosphate) and protease inhibitors (1 μg/ml aprotinin, 1 μg/ml leupeptin, and 10 mM PMSF). Lysates were spun down at 13,000 *g* for 10 min, and 500 μg of total lysate was used to immunoprecipitate p190RhoGAP with a mAb against it for 2 h. Protein G–Sepharose was added for another 2 h, and immunocomplexes were washed five times and run on an SDS-PAGE. Tubulin, phosphorylated, and total p190RhoGAP bands were quantified with ImageGauge 4.0 (FujiFilm).

Statistical analysis

Statistical significance was determined using a *t* test with OriginPro7 software (OriginLab Co.). P values < 0.05 were considered significant.

Online supplemental material

Fig. S1 shows that absence of caveolin-1 does not delay cell spreading. Fig. S2 shows that constitutively active Rho and dominant-negative mutants of Rac and Cdc42 restore normal polarity in Cav1$^{-/-}$ fibroblasts. Fig. S3 shows that a dominant-negative p190RhoGAP construct rescues polarity in Cav1$^{-/-}$ fibroblasts. Fig. S4 demonstrates that Src inhibition and p190RhoGAP knockdown in Cav1$^{-/-}$ MEFs restore the WT morphology pattern. Fig. S5 shows that total and tyrosine phosphorylated p190RhoGAP are elevated in Cav1$^{-/-}$ MEFs. Video 1 shows adhesion turnover in WT MEFs. Video 2 shows adhesion turnover in Cav1$^{-/-}$ MEFs. Video 3 shows protrusion–retraction analysis in WT MEFs. Video 4 shows protrusion–retraction analysis in Cav1$^{-/-}$ MEFs. Video 5 displays random migration of WT MEFs. Video 6 demonstrates random migration of Cav1$^{-/-}$ MEFs. Video 7 shows random migration of Cav1$^{-/-}$ MEFs reconstituted with Cav1. Video 8 shows in vitro wound-healing assays in WT MEFs. Video 9 shows in vitro wound-healing assays in Cav1$^{-/-}$ MEFs. Video 10 demonstrates in vitro wound-healing assays in Cav1$^{-/-}$ MEFs reconstituted with Cav1. Online supplemental material is available at http://www.jcb.org/cgi/content/full/jcb.200701006/DC1.

We thank Michael P. Lisanti and Richard G.W. Anderson for MEFs and thymus fibroblasts from Cav1$^{-/-}$ and Cav1$^{+/+}$ littermate mice, respectively, and Keith Burridge for GFP-p190 R1283A. We are grateful to A. Cerezo, M. Guadamillas, and I. Flores for advice and assistance in in vivo wound-healing experiments; J.C. García (Research Computing, Centro Nacional de Investigaciones Cardiovasculares) for software assistance; and M.C. Montoya, A.G. Arroyo, and J.M. Redondo for critical reading of the manuscript.

This work was supported by the Spanish Ministry of Science and Education (grants SAF2005-00493 and GEN2003-20239-C06-04 to M.A. del Pozo), a predoctoral fellowship (BEF-2003-2712 to A. Grande-García), the Ramón y Cajal Program (to A. Echarri and M.A. del Pozo), and the European Union (Marie Curie International Reintegration grant MIRG-CT-2005-016427 to M.A. del Pozo). M.A. del Pozo is an EMBO Young Investigator and the recipient of an EURYI (European Young Investigator) award.

Submitted: 2 January 2007
Accepted: 23 April 2007

References

Arthur, W.T., and K. Burridge. 2001. RhoA inactivation by p190RhoGAP regulates cell spreading and migration by promoting membrane protrusion and polarity. *Mol. Biol. Cell.* 12:2711–2720.

Arthur, W.T., L.A. Petch, and K. Burridge. 2000. Integrin engagement suppresses RhoA activity via a c-Src-dependent mechanism. *Curr. Biol.* 10:719–722.

Beardsley, A., K. Fang, H. Mertz, V. Castranova, S. Friend, and J. Liu. 2005. Loss of caveolin-1 polarity impedes endothelial cell polarization and directional movement. *J. Biol. Chem.* 280:3541–3547.

Brouns, M.R., S.F. Matheson, and J. Settleman. 2001. p190 RhoGAP is the principal Src substrate in brain and regulates axon outgrowth, guidance and fasciculation. *Nat. Cell Biol.* 3:361–367.

Burridge, K., and K. Wennerberg. 2004. Rho and Rac take center stage. *Cell.* 116:167–179.

Cao, H., W.E. Courchesne, and C.C. Mastick. 2002. A phosphotyrosine-dependent protein interaction screen reveals a role for phosphorylation of caveolin-1 on tyrosine 14: recruitment of C-terminal Src kinase. *J. Biol. Chem.* 277:8771–8774.

Carragher, N.O., and M.C. Frame. 2004. Focal adhesion and actin dynamics: a place where kinases and proteases meet to promote invasion. *Trends Cell Biol.* 14:241–249.

de Rooij, J., A. Kerstens, G. Danuser, M.A. Schwartz, and C.M. Waterman-Storer. 2005. Integrin-dependent actomyosin contraction regulates epithelial cell scattering. *J. Cell Biol.* 171:153–164.

del Pozo, M.A., M. Vicente-Manzanares, R. Tejedor, J.M. Serrador, and F. Sánchez-Madrid. 1999. Rho GTPases control migration and polarization of adhesion molecules and cytoskeletal ERM components in T lymphocytes. *Eur. J. Immunol.* 29:3609–3620.

del Pozo, M.A., L.S. Price, N.B. Alderson, X.D. Ren, and M.A. Schwartz. 2000. Adhesion to the extracellular matrix regulates the coupling of the small GTPase Rac to its effector PAK. *EMBO J.* 19:2008–2014.

del Pozo, M.A., N. Balasubramanian, N.B. Alderson, W.B. Kiosses, A. Grande-Garcia, R.G. Anderson, and M.A. Schwartz. 2005. Phospho-caveolin-1 mediates integrin-regulated membrane domain internalization. *Nat. Cell Biol.* 7:901–908.

DeMali, K.A., K. Wennerberg, and K. Burridge. 2003. Integrin signaling to the actin cytoskeleton. *Curr. Opin. Cell Biol.* 15:572–582.

Drab, M., P. Verkade, M. Elger, M. Kasper, M. Lohn, B. Lauterbach, J. Menne, C. Lindschau, F. Mende, F.C. Luft, et al. 2001. Loss of caveolae, vascular dysfunction, and pulmonary defects in caveolin-1 gene-disrupted mice. *Science.* 293:2449–2452.

Fukuyama, T., H. Ogita, T. Kawakatsu, T. Fukuhara, T. Yamada, T. Sato, K. Shimizu, T. Nakamura, M. Matsuda, and Y. Takai. 2005. Involvement of the c-Src-Crk-C3G-Rap1 signaling in the nectin-induced activation of Cdc42 and formation of adherens junctions. *J. Biol. Chem.* 280:815–825.

Galvez, B.G., S. Matias-Roman, M. Yanez-Mo, M. Vicente-Manzanares, F. Sanchez-Madrid, and A.G. Arroyo. 2004. Caveolae are a novel pathway for membrane-type 1 matrix metalloproteinase traffic in human endothelial cells. *Mol. Biol. Cell.* 15:678–687.

Ge, S., and J.S. Pachter. 2004. Caveolin-1 knockdown by small interfering RNA suppresses responses to the chemokine monocyte chemoattractant protein-1 by human astrocytes. *J. Biol. Chem.* 279:6688–6695.

Geiger, B., and A. Bershadsky. 2001. Assembly and mechanosensory function of focal contacts. *Curr. Opin. Cell Biol.* 13:584–592.

Glenney, J.R., and L. Zokas. 1989. Novel tyrosine kinase substrates from Rous sarcoma virus-transformed cells are present in the membrane skeleton. *J. Cell Biol.* 108:2401–2408.

Gonzalez, E., A. Nagiel, A.J. Lin, D.E. Golan, and T. Michel. 2004. Small interfering RNA-mediated down-regulation of caveolin-1 differentially modulates signaling pathways in endothelial cells. *J. Biol. Chem.* 279:40659–40669.

Hakak, Y., and G.S. Martin. 1999. Ubiquitin-dependent degradation of active Src. *Curr. Biol.* 9:1039–1042.

Hassan, G.S., T.M. Williams, P.G. Frank, and M.P. Lisanti. 2006. Caveolin-1-deficient aortic smooth muscle cells show cell autonomous abnormalities in proliferation, migration, and endothelin-based signal transduction. *Am. J. Physiol. Heart Circ. Physiol.* 290:H2393–H2401.

Huttenlocher, A. 2005. Cell polarization mechanisms during directed cell migration. *Nat. Cell Biol.* 7:336–337.

Isshiki, M., J. Ando, K. Yamamoto, T. Fujita, Y. Ying, and R.G. Anderson. 2002. Sites of Ca^{2+} wave initiation move with caveolae to the trailing edge of migrating cells. *J. Cell Sci.* 115:475–484.

Kawakatsu, T., H. Ogita, T. Fukuhara, T. Fukuyama, Y. Minami, K. Shimizu, and Y. Takai. 2005. Vav2 as a Rac-GDP/GTP exchange factor responsible for the nectin-induced, c-Src- and Cdc42-mediated activation of Rac. *J. Biol. Chem.* 280:4940–4947.

Kurokawa, K., and M. Matsuda. 2005. Localized RhoA activation as a requirement for the induction of membrane ruffling. *Mol. Biol. Cell.* 16:4294–4303.

Le Lay, S., and T.V. Kurzchalia. 2005. Getting rid of caveolins: phenotypes of caveolin-deficient animals. *Biochim. Biophys. Acta.* 1746:322–333.

Li, Z., M. Hannigan, Z. Mo, B. Liu, W. Lu, Y. Wu, A.V. Smrcka, G. Wu, L. Li, M. Liu, et al. 2003. Directional sensing requires G beta gamma-mediated PAK1 and PIX alpha-dependent activation of Cdc42. *Cell.* 114:215–227.

Machesky, L.M., and A. Hall. 1997. Role of actin polymerization and adhesion to extracellular matrix in Rac- and Rho-induced cytoskeletal reorganization. *J. Cell Biol.* 138:913–926.

Meili, R., and R.A. Firtel. 2003. Two poles and a compass. *Cell.* 114:153–156.

Meng, W., M. Numazaki, K. Takeuchi, Y. Uchibori, Y. Ando-Akatsuka, M. Tominaga, and T. Tominaga. 2004. DIP (mDia interacting protein) is a key molecule regulating Rho and Rac in a Src-dependent manner. *EMBO J.* 23:760–771.

Miyamoto, Y., J. Yamauchi, and H. Itoh. 2003. Src kinase regulates the activation of a novel FGD-1-related Cdc42 guanine nucleotide exchange factor in the signaling pathway from the endothelin A receptor to JNK. *J. Biol. Chem.* 278:29890–29900.

Navarro, A., B. Anand-Apte, and M.O. Parat. 2004. A role for caveolae in cell migration. *FASEB J.* 18:1801–1811.

Nimnual, A.S., L.J. Taylor, and D. Bar-Sagi. 2003. Redox-dependent downregulation of Rho by Rac. *Nat. Cell Biol.* 5:236–241.

Nishiya, N., W.B. Kiosses, J. Han, and M.H. Ginsberg. 2005. An alpha4 integrin-paxillin-Arf-GAP complex restricts Rac activation to the leading edge of migrating cells. *Nat. Cell Biol.* 7:343–352.

Noren, N.K., W.T. Arthur, and K. Burridge. 2003. Cadherin engagement inhibits RhoA via p190RhoGAP. *J. Biol. Chem.* 278:13615–13618.

Pankov, R., Y. Endo, S. Even-Ram, M. Araki, K. Clark, E. Cukierman, K. Matsumoto, and K.M. Yamada. 2005. A Rac switch regulates random versus directionally persistent cell migration. *J. Cell Biol.* 170:793–802.

Parat, M.O., B. Anand-Apte, and P.L. Fox. 2003. Differential caveolin-1 polarization in endothelial cells during migration in two and three dimensions. *Mol. Biol. Cell.* 14:3156–3168.

Parton, R.G., M. Hanzal-Bayer, and J.F. Hancock. 2006. Biogenesis of caveolae: a structural model for caveolin-induced domain formation. *J. Cell Sci.* 119:787–796.

Pear, W.S., J.P. Miller, L. Xu, J.C. Pui, B. Soffer, R.C. Quackenbush, A.M. Pendergast, R. Bronson, J.C. Aster, M.L. Scott, and D. Baltimore. 1998. Efficient and rapid induction of a chronic myelogenous leukemia-like myeloproliferative disease in mice receiving P210 bcr/abl-transduced bone marrow. *Blood.* 92:3780–3792.

Pertz, O., L. Hodgson, R.L. Klemke, and K.M. Hahn. 2006. Spatiotemporal dynamics of RhoA activity in migrating cells. *Nature.* 440:1069–1072.

Podar, K., R. Shringarpure, Y.T. Tai, M. Simoncini, M. Sattler, K. Ishitsuka, P.G. Richardson, T. Hideshima, D. Chauhan, and K.C. Anderson. 2004. Caveolin-1 is required for vascular endothelial growth factor-triggered multiple myeloma cell migration and is targeted by bortezomib. *Cancer Res.* 64:7500–7506.

Radel, C., and V. Rizzo. 2005. Integrin mechanotransduction stimulates caveolin-1 phosphorylation and recruitment of Csk to mediate actin reorganization. *Am. J. Physiol. Heart Circ. Physiol.* 288:H936–H945.

Raftopoulou, M., and A. Hall. 2004. Cell migration: Rho GTPases lead the way. *Dev. Biol.* 265:23–32.

Razani, B., J.A. Engelman, X.B. Wang, W. Schubert, X.L. Zhang, C.B. Marks, F. Macaluso, R.G. Russell, M. Li, R.G. Pestell, et al. 2001. Caveolin-1 null mice are viable but show evidence of hyperproliferative and vascular abnormalities. *J. Biol. Chem.* 276:38121–38138.

Ren, X.D., W.B. Kiosses, D.J. Sieg, C.A. Otey, D.D. Schlaepfer, and M.A. Schwartz. 2000. Focal adhesion kinase suppresses Rho activity to promote focal adhesion turnover. *J. Cell Sci.* 113:3673–3678.

Ridley, A.J., M.A. Schwartz, K. Burridge, R.A. Firtel, M.H. Ginsberg, G. Borisy, J.T. Parsons, and A.R. Horwitz. 2003. Cell migration: integrating signals from front to back. *Science.* 302:1704–1709.

Rottner, K., A. Hall, and J.V. Small. 1999. Interplay between Rac and Rho in the control of substrate contact dynamics. *Curr. Biol.* 9:640–648.

Sánchez-Madrid, F., and M.A. del Pozo. 1999. Leukocyte polarization in cell migration and immune interactions. *EMBO J.* 18:501–511.

Sander, E.E., J.P. ten Klooster, S. van Delft, R.A. van der Kammen, and J.G. Collard. 1999. Rac downregulates Rho activity: reciprocal balance between both GTPases determines cellular morphology and migratory behavior. *J. Cell Biol.* 147:1009–1022.

Servitja, J.M., M.J. Marinissen, A. Sodhi, X.R. Bustelo, and J.S. Gutkind. 2003. Rac1 function is required for Src-induced transformation: evidence of a role for Tiam1 and Vav2 in Rac activation by Src. *J. Biol. Chem.* 278:34339–34346.

Shaul, P.W., and R.G. Anderson. 1998. Role of plasmalemmal caveolae in signal transduction. *Am. J. Physiol.* 275:L843–L851.

Sheetz, M.P., D. Felsenfeld, C.G. Galbraith, and D. Choquet. 1999. Cell migration as a five-step cycle. *Biochem. Soc. Symp.* 65:233–243.

Singer, A.J., and R.A. Clark. 1999. Cutaneous wound healing. *N. Engl. J. Med.* 341:738–746.

Sonveaux, P., P. Martinive, J. DeWever, Z. Batova, G. Daneau, M. Pelat, P. Ghisdal, V. Gregoire, C. Dessy, J.L. Balligand, and O. Feron. 2004. Caveolin-1 expression is critical for vascular endothelial growth factor-induced ischemic hindlimb collateralization and nitric oxide-mediated angiogenesis. *Circ. Res.* 95:154–161.

Stahlhut, M., and B. van Deurs. 2000. Identification of filamin as a novel ligand for caveolin-1: evidence for the organization of caveolin-1-associated membrane domains by the actin cytoskeleton. *Mol. Biol. Cell.* 11:325–337.

Tu, S., W.J. Wu, J. Wang, and R.A. Cerione. 2003. Epidermal growth factor-dependent regulation of Cdc42 is mediated by the Src tyrosine kinase. *J. Biol. Chem.* 278:49293–49300.

Valasek, M.A., J. Weng, P.W. Shaul, R.G. Anderson, and J.J. Repa. 2005. Caveolin-1 is not required for murine intestinal cholesterol transport. *J. Biol. Chem.* 280:28103–28109.

Vicente-Manzanares, M., D.J. Webb, and A.R. Horwitz. 2005. Cell migration at a glance. *J. Cell Sci.* 118:4917–4919.

Wary, K.K., A. Mariotti, C. Zurzolo, and F.G. Giancotti. 1998. A requirement for caveolin-1 and associated kinase Fyn in integrin signaling and anchorage-dependent cell growth. *Cell.* 94:625–634.

Wehrle-Haller, B., and B. Imhof. 2002. The inner lives of focal adhesions. *Trends Cell Biol.* 12:382–389.

Wei, Y., X. Yang, Q. Liu, J.A. Wilkins, and H.A. Chapman. 1999. A role for caveolin and the urokinase receptor in integrin-mediated adhesion and signaling. *J. Cell Biol.* 144:1285–1294.

Woodman, S.E., A.W. Ashton, W. Schubert, H. Lee, T.M. Williams, F.A. Medina, J.B. Wyckoff, T.P. Combs, and M.P. Lisanti. 2003. Caveolin-1 knockout mice show an impaired angiogenic response to exogenous stimuli. *Am. J. Pathol.* 162:2059–2068.

Xu, J., F. Wang, A. Van Keymeulen, P. Herzmark, A. Straight, K. Kelly, Y. Takuwa, N. Sugimoto, T. Mitchison, and H.R. Bourne. 2003. Divergent signals and cytoskeletal assemblies regulate self-organizing polarity in neutrophils. *Cell.* 114:201–214.

Zhang, W., B. Razani, Y. Altschuler, B. Bouzahzah, K.E. Mostov, R.G. Pestell, and M.P. Lisanti. 2000. Caveolin-1 inhibits epidermal growth factor-stimulated lamellipod extension and cell migration in metastatic mammary adenocarcinoma cells (MTLn3). Transformation suppressor effects of adenovirus-mediated gene delivery of caveolin-1. *J. Biol. Chem.* 275:20717–20725.